Caelus - A Tour through the Main Asteroid Belt

Christina Athanasiadou, Elodie Monique Bourens, Susana Carneiro, Louis Carton, Antea Carine Doriot, Moritz Goldmann, Vanessa Helperstorfer, Jaap Jorritsma, Matouš Moravec, Carmen Naletto, Andrés Pintado Lázaro, Jose Enrique Prósper Álvarez, Alan Sajan, Fabian Seel, Alina Vassiljeva

July 16, 2025

Abstract

The Caelus mission aims to explore multiple asteroids in the Main Asteroid Belt to address the fundamental question: What causes the spectral diversity observed across asteroids in the main belt? Designed as a multi-target rendezvous and impactor mission, Caelus uses a combination of electric and chemical propulsion to sequentially visit and investigate five asteroids of different types. The spacecraft carries a suite of scientific instruments, including a hyperspectral imager, thermal infrared camera, laser altimeter, and radio science instrument, to conduct surface mapping, compositional analysis, and subsurface characterization. An onboard impactor module allows for direct investigation of the mechanical properties and buried material of selected targets. The collected data will support scientific objectives related to solar system formation, asteroid material properties, and planetary defense. The mission design follows a scalable and modular approach, with the ability to reduce or extend the scope depending on technical and budgetary considerations. Caelus is planned for launch aboard an Ariane 64 vehicle within ESA's L-class mission program.

1 Introduction

1.1 Solar System Formation and the Asteroid main belt

The formation and early evolution of the Solar System occurred approximately 4.56 billion years ago, beginning with the gravitational collapse of a dense region within an interstellar molecular cloud. This event led to the creation of the solar nebula, a rotating disk of gas and dust surrounding the proto-Sun. Within this protoplanetary disk, solid particles underwent several growth processes, likely seeded by streaming instabilities, including coagulation, settling, and gravitational accumulation, ultimately leading to the formation of planetesimals and eventually terrestrial planets [20, 44].

Several models have been proposed to explain the structure and compositional gradients observed in the Solar System. The classical model suggests a gradual, local accretion of planetesimals within a temperature gradient across the nebula that influences volatile condensation, resulting in refractory-rich inner regions and volatile-rich outer regions. However, this model does not fully explain the observed distribution and mixing of small bodies. More recent dynamical models, such as the Nice Model and the Grand Tack Hypothesis [38, 41], propose large-scale planetary migration and dynamical instabilities. These models suggest that Jupiter and Saturn migrated significantly during the early evolution of the Solar System, perturbing and redistributing small bodies and causing extensive radial mixing of material formed at different heliocentric distances [25].

The asteroid main belt, located between approximately 2.0 and 3.3 AU [20] from the Sun, contains a vast collection of rocky remnants and thermally processed bodies. These objects, many of which are relics from the early stages of planetary formation, did not fully accrete into planets. As such, they preserve invaluable information about the primordial Solar System materials. The compositional and dynamical diversity observed among the main belt asteroids provides evidence of both localized thermal evolution, collisions, and large-scale transport processes. The main belt thus serves as an archive, capturing the dynamic physical and chemical processes that have shaped the Solar System.

1.2 Asteroid Composition and Classification

Asteroids, primarily located in the main belt but also present in near-Earth orbits and beyond Neptune, are classified on the basis of their reflectance spectra in the visible and near-infrared range that can be recorded in ground-based measurements. While these spectra are directly related to the asteroid's surface composition, the compositional information that can be derived from them is limited. By investigating meteorite samples with similar spectral properties, Earth-based measurements can help infer more details on the different spectral classes. C-class asteroids are considered the most pristine bodies from the early Solar System and the most primitive in composition, having undergone minimal thermal alteration, preserving the earliest Solar System materials [14]. More evolved chondrites have experienced low-temperature aqueous alteration (<300 °C) or thermal metamorphism (400 to 950 °C) [16]. Chondrites account for more than 90% of meteorite falls [39]. Other spectral types, such as S-, E-, and M-class asteroids, have experienced partial melting or complete differentiation, producing achondrite, stony-iron, and iron meteorites, which make up approximately 10% of meteorite falls. D- and P-type asteroids, mainly found in the outer belt, have low albedo and red-sloped spectra. Although they are thought to contain organic-rich silicates and carbon compounds, no definitive meteorite analogs have been found for them as of the writing of this report. Their spectral similarities to cometary materials suggest a potential link to volatile-rich bodies [39].

1.3 Physical Properties and Internal Structure

From Earth-based observations, the internal structure of asteroids remains poorly constrained due to limitations of remote sensing techniques, which primarily probe surface materials. Bulk densities can be estimated from mass and volume measurements, which are derived from gravitational perturbations and shape modeling using light curves, radar, and stellar occultation [36]. Additionally, the thermal inertia of the surface regolith can be used to estimate surface roughness and grain size distribution [23].

In in situ measurements, the volume can be determined with high accuracy using stereophotoclinometry [1], and investigations

of the higher degree coefficients of the gravity field can provide constraints for inhomogeneous mass distribution [45]. Furthermore, thermal infrared imaging of the diurnal thermal cycle of boulders on the asteroid surface provides insight into their thermal inertia and microporosity [25]. These properties can be related to the porosity of the interior of the parent body [25].

1.4 Past Missions

Over the past three decades, space missions have significantly advanced our understanding of asteroids. Flyby missions like Galileo (1989), which encountered the S-type asteroids Gaspra and Ida [5], and the mission NEAR Shoemaker (1996), which studied the C-type asteroid Mathilde and later orbited and landed on Sw-type Eros, provided the first direct observations of asteroid surfaces, revealing cratered and heterogeneous terrains [31]. Sample return missions such as those of Hayabusa (Itokawa, S-type in 2005) confirmed the rubble-pile nature of some asteroids and directly linked S-types to ordinary chondrites [40]. ESA's Rosetta mission conducted flybys of Šteins (X-type) in 2008 and Lutetia (X-type) in 2010 [37], generating high-resolution data, while NASA's Dawn orbiter investigated the bodies Vesta (V-type) and Ceres (C-type) in 2011 and 2015 respectively, uncovering evidence of internal differentiation and cryovolcanism. Hayabusa2 (C-type Ryugu in 2018) [42] and OSIRIS-REx (B-type Bennu in 2018) [22] returned pristine carbonaceous material with unique isotopic signatures that was rich in organics, hydrated minerals. NASA's DART mission demonstrated the feasibility of kinetic impact for planetary defense by altering the orbit of Dimorphos, the moon of the binary asteroid Didymos [6].

1.5 Ongoing and Future Missions

Current missions include NASA's Lucy, en route to study Jupiter Trojans [8], and Psyche, targeting the potentially metal-rich asteroid Psyche [9]. Future missions such as JAXA's DESTINY+, ESA's Hera, and CNSA's Tianwen-2 aim to expand the survey of asteroid types through flybys, orbiters, and returned samples. These missions demonstrate the ongoing effort to uncover the origin and evolution of small Solar System bodies using ever more advanced technology and observational scope.

2 Science Motivation for Caelus

2.1 Knowledge Gaps and Challenges

Asteroids represent the preserved building blocks of planetary formation, yet their origin and evolution remain only partially understood. Although ground-based surveys and targeted space missions have revealed the spectral and morphological diversity of these bodies, key aspects of their internal physical and compositional structure, as well as their surface evolution , remain poorly constrained. Existing data suggest that some asteroids have undergone significant thermal processing, aqueous alteration, or even partial differentiation, while others retain more primitive features [17].

2.2 Target Diversity and Scientific Opportunity

The current sample of asteroids explored in - situ is limited in the diversity of spectral classes, the position of the asteroids within the main belt. Furthermore, only two bodies were closely investigated in rendezvous, whereas all other missions at the time of writing were flyby missions, and thus were strongly limited in their close-range observations [33]. Caelus addresses these limitations by exploring five main belt asteroids, selected to expand in situ observations to previously unexplored spectral types, thus providing insights into their parent bodies and the processes of thermal and compositional evolution that shaped them.

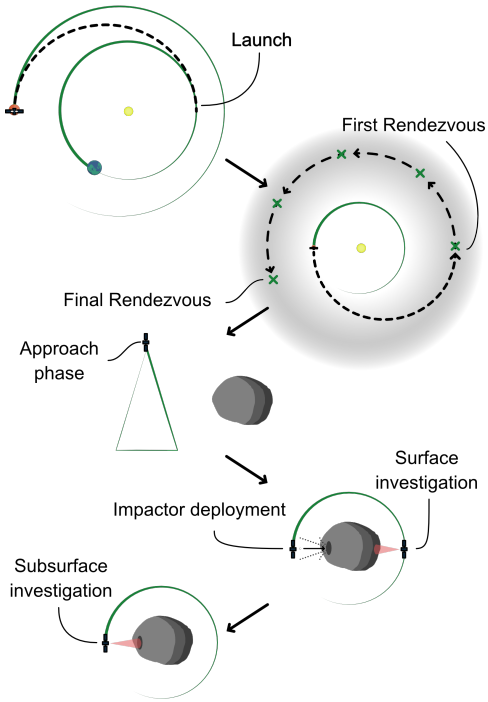

Figure 1. Schematic of the mission architecture. The spacecraft is launched from Earth, performs a transfer trajectory towards the asteroid belt, and initiates a series of rendezvous maneuvers with selected target asteroids. Each rendezvous includes an approach phase followed by close-proximity operations and surface investigations. The mission concludes with a final rendezvous before end-of-life operations.

By combining measurements of morphologic features, mineral composition, thermal properties, elemental abundances, both for the surface and subsurface material, as well as volume and mass of the bulk of the asteroid, Caelus will produce a multidimensional data set that links surface properties with internal properties. This holistic approach is necessary to understand not just what these bodies are made of but how their structures and compositions evolved over time, and will be valuable for the interpretation of ground-based observations.

Caelus will investigate evolutionary signatures across its targets, including regolith distribution, impact cratering histories, and thermal properties, which provide information about porosity and formation age [25]. Crucially, the mission's approach enables comparative analysis across asteroid classes, not only from surface features, but also from subsurface layers revealed in craters that are deliberately produced by impactors. This provides direct access to material shielded from space weathering, offering the rare opportunity to examine primitive subsurface material in situ and establish links with meteorite analogs observed in laboratory collections.

2.3 Scientific Objectives and Requirements

Although a lot of work has been done to relate the different spectral classes to meteorites and thus to possible compositions as

pointed out in Section 1.2, it is still largely unclear how local physical and morphological properties relate to the measured spectra. Previous missions, such as the Hayabusa2 mission to asteroid Ryugu, found e.g., fundamental differences between the expected and observed regolith size distribution [14]. The overarching goal of the proposed mission is to support closing this gap formulated as the question "What causes the spectral diversity across the asteroids of the main belt?". Answering this question includes understanding the current state, how the asteroid has evolved, and where it originated.

To investigate the formation and evolution of asteroids in the main belt, the mission aims to constrain both the surface and subsurface compositions, as well as their physical properties, with a single spacecraft, see Figure 1. Table 1 presents the scientific objectives (SO) and their traceability to scientific requirements, observables, and measurement methods. In order to expand the available in situ measurements to a significantly larger set of spectral classes while staying within feasibility limits determined by external factors such as financial cost and launch vehicle availability, Caelus will investigate a suite of 5 different asteroids, while covering at least 3 different spectral classes, with the goal to investigate at least 3 previously unexplored spectral classes. Note that the complete requirements matrix, including the derivation of instrument requirements, is not part of this document, but is detailed in a separate document and will be made available upon request.

2.4 SO 1: The subsurface composition and structure of a suite of asteroids of different types along the main belt shall be investigated to inform simulations that study the formation history of their parent bodies.

Most smaller bodies in the main belt are believed to be single or multiple re-accreted fragments of initially larger parent bodies that underwent catastrophic collisions [4]. While various compaction, heating and differentiation processes are thought to have happened during the formation of different parent bodies, the boulders on the surface of current asteroids are thought to be fragments from mentioned collisions which have not been significantly compacted after the parent body formation and are thus remnants of early Solar System processes [4, 26]. Furthermore, current asteroid surfaces are thought to be altered by weathering of the surface material, making it impossible to infer the pristine composition of the body [24]. For each visited asteroid, the proposed mission shall determine the bulk density, the surface boulder microporosity, as well as the mineral and elemental composition on and below the weathered surface. The bulk density and boulder microporosity can be used to evaluate the structural heterogeneity of the investigated asteroid, whether it consists of fragments from the same regions within its parent body, from different regions of a compacted or differentiated body, or potentially from different parent bodies [26]. The unweathered mineral and elemental composition sets constrains on the hydrothermal conditions during the parent body formation [26]. Combined, more information about the formation history, the time after CAI formation (Ca-Al-rich Inclusions, the oldest dated minerals in the solar system [43]), and the parent body size can be estimated.

2.5 SO 2: Evolutionary changes of the composition and structure of a suite of asteroids of different types along the main belt shall be studied.

Small airless bodies in our Solar System are subjected to several processes that alter their composition and morphology, including space weathering and gardening. Space weathering refers to a collection of processes, e.g., meteoritic impacts, cosmic radiation, and solar wind ion implantation. These processes can lead to compaction, heating, and the formation of nanophase iron from vapor deposition of heated silicates. The latter process is an important driver for changes of the spectral slope on the surface of the Moon, but poorly constrained for the surface of asteroids, where meteoritic impacts seem to be the dominating process for changes in the spectral slope [18, 46]. Furthermore, large and rapid diurnal temperature changes can lead to significant thermal stresses on boulders, leading to the formation of cracks, and, together with meteoritic impacts, to the production of nanometer to decimeter-sized regolith [29, 10, 32]. Surface weathering is counteracted by the turnover of surface and near subsurface material in a process known as gardening. The processes driving gardening include gravitational interactions with other bodies, and also meteoritic impacts. The depth of the gardening processes is still unclear and subject of recent studies [24]. The proposed mission shall observe the surface of different asteroids to characterize features and morphological structures resulting from those effects. Furthermore, observations of the surface and subsurface reflection slopes will be compared to investigate spectral changes induced by space weathering. The surface of different asteroids shall be compared with each other to investigate possible correlations between different spectral classes and different evolutionary histories.

2.6 Instrumentation

To meet the mission scientific requirements, the payload consists of a set of imagers, a radio science instrument, and a gamma-ray neutron detector. The instrumentation design will be better defined during Caelus Phase B, while their development and testing will be carried out during the mission Phases C and D.
As for this proposal, the instrumentation presented is based on heritage that proves the feasibility of the instrument requirements. In particular, the instruments considered and the respective scientific requirements are as follows.

A **Narrow Angle Camera (NAC)** for detailed mapping of regolith and boulder size distribution and morphology is being adopted. The instrument requirement is a minimum spatial resolution of 2.5 cm/pixel. For this, a NAC derived from the modified Ritchey-Chrétien telescope, JANUS, for the JUICE mission, can be used. With an aperture of 100 mm, a focal length of 467 mm, and a pixel size of 7 µm [28], the instrument reaches a spatial resolution of ≃2 cm/px at 1 km altitude. Its narrow field of view (1.72° × 1.29°) and sensitivity across 340 to 1080 nm support the analysis of fine-scale geological features needed for porosity estimation and thermal modeling, fulfilling the instrument requirements.

A **Wide Angle Camera (WAC)** with minimum spatial resolution of 2.5 cm/pixel is required for global surface mapping, context imaging, and detailed shape modeling, as well as initial shape modeling during approach.
Basing Caelus WAC on Dawn Framing Camera (FC) [19], this resolution can be achieved. Operating in the 400 to 1050 nm spectral range with a field of view of 5.5° ×5.5°, FC acquires surface mor-

Table 1. Traceability matrix for Science Objectives including requirements, methods, and observables.

Scientific Objectives	Scientific Requirements	Observables	Methods
SO1: The subsurface composition and structure of a suite of asteroids of different types along the main belt shall be investigated to inform simulations that study the formation history of their parent bodies.	**SO-1.1:** Determine the bulk density.	Asteroid Shape Asteroid Mass	VIS Camera (WAC), TIR Imager HGA
	SO-1.2: Determine the boulder microporosity.	Boulder Size Boulder Thermal Inertia	VIS Camera (NAC) TIR Imager
	SO-1.3: Determine the subsurface mineral composition.	Fresh Material Excavation Mineral Components	Impactor Hyperspectral Camera
	SO-1.4: Determine the (sub-) surface elemental composition.	Elemental Composition	γ-ray and Neutron Emission Detection
SO2: Evolutionary changes of composition and structure of a suite of asteroids of different types along the main belt shall be studied.	**SO-2.1:** Determine the surface mineral composition.	Mineral composition	Hyperspectral Camera
	SO-2.2: Determine the surface mineral distribution.	Mineral composition	Hyperspectral Camera
	SO-2.3: Determine the crater size distribution.	Crater size	VIS Camera (WAC)
	SO-2.4: Determine the crater spatial density.	Crater density	VIS Camera (WAC)
	SO-2.5: Determine the surface regolith size distribution.	Regolith Size	VIS Camera (NAC)
	SO-2.6: Observe surface features linked to, e.g., weathering and erosion.	Boulder surface features Boulder thermal cycling Regolith distribution	VIS Camera (NAC) TIR Imager VIS Camera (NAC)
	SO-2.7: Determine surface reddening.	Subsurface reflectance spectrum Surface reflectance spectrum	Hyperspectral Camera Hyperspectral Camera

phology data at spatial resolution of 9.37 cm/pixel at 1 km.

A **Radio Science Instrument (RSI)** adapted from Hera's X-DST unit [13] is included to measure the asteroid's gravitational field by tracking Doppler shifts in the spacecraft's velocity. The instrument must detect velocity changes smaller than or equal to $3\,\mu m\,s^{-1}$ over 1000 seconds, which corresponds to the gravitational acceleration produced by a spherical body with a radius of 250 m and a bulk density of 1.3 g/cm^3 at a distance of 10 km. When combined with volume data derived from the WAC shape model, this enables the estimation of the asteroid's bulk density.

The **Hyperspectral Imager**, adapted from MMX's MIRS [3], is a push-broom spectrometer designed for compositional analysis, surface mineral mapping, and space weathering studies. It covers the 0.9-3.6 µm spectral range with 20 nm spectral resolution to detect the absorption features of both altered and unaltered minerals. To meet Caelus's scientific objectives, the spatial resolution must be improved from 22.5 cm/pixel to at least 12.8 cm/pixel.

The **Thermal InfraRed Imager (TIRI)**, based on the Hera mission design [27], employs an uncooled microbolometer array covering the 700 to 1400 nm range and measuring temperatures between 150-450 K. To assess the diurnal temperature evolution of individual boulders-including night-side temperatures down to 80 K at 3 AU [**?**]-a spatial resolution of at least 12.8 cm/pixel is required, necessitating optimization of TIRI's optical system.

A **Gamma-ray and Neutron Detector (GRaND)** to determine the elemental composition of the asteroid's subsurface and distinguish between compositional end members of minerals found in the reflectance spectra is required. The instrument should be able to measure major rock-forming elements (e.g., Si, Mg, Fe, Al and Ca) as well as volatiles (e.g., H and C). The GRaND, will be built on Dawn mission heritage [30], which allows insight into geochemical layering and the presence of hydrated or primitive materials to depths of ~1 m.

Finally, the mission adopts an **impactor** to sample the asteroid subsurface by generating small artificial craters. The goal is to expose fresh material by creating $\geq$ 20 cm deep craters with a 0.75 m radius of affectance, without destabilizing the spacecraft or interfering with the instruments. This enables high-resolution post-impact observations by NAC, WAC, and TIR imagers. The projectile parameters (Ø 4 cm, 270 g, 450 m/s) are derived from an empirical formula developed using Hayabusa2 impact data [2], requiring a new design (TRL 3), not previously tested. It consists of six self-contained ejector units, each embedding a liner, barrel, internal electronics, and 15.7 g of HMX explosive, enclosed in a blast and thermally resistant casing. Upon activation, each ejector launches a hollow zirconium projectile (chosen for strength and easy identification, as zirconium is absent from asteroid material). Shielding, mechanical decoupling, and center-of-mass mounting are used to ensure safe operation without perturbing the spacecraft (S/C) or its measurements [34].

3 Mission Design

3.1 Mission Timeline

The mission is planned to launch on 24 October 2041 aboard an Ariane 64 launch vehicle, targeting a hyperbolic excess velocity of approximately 3.6 km/s. Following launch, the spacecraft will execute a 15.5-month low-thrust transfer to Mars, where a gravity assist will be used to increase heliocentric velocity and adjust the orbital inclination. This maneuver is required to match the ~20° inclination of the first target asteroid relative to the ecliptic plane. After the Mars flyby, the spacecraft will continue on a 5.2-year interplanetary cruise to reach the first asteroid, Einstein, 1973 EB, located at a heliocentric distance of 1.93 AU, with an approach velocity below 1 m/s.

3.2 Trajectory and Orbit

Following the completion of the interplanetary transfer in 2048, for the nominal plan, the asteroid transfer, also called "asteroid hopping", and the scientific phases will start. This phase consists

of two separate sequences. The first one, relative to the Sun, allows the spacecraft to go from one asteroid to another, and the other sequence, to perform the scientific operation once arrived at each target, which consists of:

1. **Arrival Phase:** Transitional phase between the asteroid hopping sequence and the scientific operation sequence. Decelerating, verification of the subsystems and payload for nominal operations.
   Duration: ~ few hours
2. **Approach Phase:** The objective of this phase is to characterize the shape and gravity field of the target for future proximity operations. We use distant hyperbolic arcs around the asteroid in order to perform a first visual and be able to compute the estimated gravity field of the asteroid.
   Duration: ~10 days
3. **Orbital Phase:** As we are staying around the asteroid for 100 days, we will stay most of this time on a **stable orbit** around the target body. For an asteroid with a diameter of ~4 km, this equilibrium between the gravity force of the asteroid and the solar radiation pressure is found to be at a distance of about 10 km. To meet the required spatial resolution, the spacecraft will operate in an orbit approximately 1 km above the surface of each asteroid. Thus, non-stable, we will use the hydrazine attitude determination and control system (ADCS) thrusters to perform the orbit-keeping. The planned orbital phase duration at each target is 100 days to ensure full surface coverage and sufficient time for data downlink.
4. **Departure Phase:** Once the scientific phase is done and all the data has been transferred to Earth we perform a check of systems before switching to the satellite transfer mode and leaving the asteroid for the next target.

Following the completion of the departure phase at each site, the estimated transfer time to the next asteroid is approximately 150 days. With five target asteroids, the total primary mission duration is projected to be around 10 years.

3.3 End of Life

If the spacecraft has sufficient remaining fuel, remains in sufficient condition to produce enough electrical energy to downlink hyperspectral data, shape models, and mass measurements, the mission could be extended beyond its primary operations. Options include rendezvous with one or more additional targets, potentially performing another impact experiment, increasing the in-orbit time for more detailed surface investigations around the final asteroid, or flybys of other nearby objects. These scenarios would significantly improve the scientific return of the mission.

Once all mission activities are completed and not enough fuel is left, we will follow ESA's guidelines regarding passivation and disposal [11]. All remaining energy sources onboard will be safely eliminated (SD-OP-03). This includes releasing leftover fuel and pressurized gases as well as fully draining the batteries. These steps ensure the spacecraft to becomes inert, preventing any risk of fragmentation after mission completion. Because the mission will be over around the main asteroid belt, multiple options for spacecraft decommissioning are possible, including a transfer to a stable disposal orbit (Distant Retrograde Orbit type) or on an intersecting trajectory with a non-critical celestial body.

3.4 Target Selection

The mission targets at least five asteroids across a minimum of three different spectral classes. Candidate bodies are limited to diameters under 5 km to reduce the likelihood of fine dust regolith on the surface, thereby improving the accuracy of temperature measurements of individual boulders. Smaller bodies also reduce the data volume required for surface mapping and shorten the duration of the science phase at each target. Additionally, their lower gravity increases the size and depth of impact craters, enhancing subsurface material analysis. A list of currently known potential targets is presented in Table 2.
The proposed primary procedure for the selection of adequate targets is to perform a survey that spectrally characterizes more asteroids within these size constraints, in order to increase the list of potential targets during following mission development phases. A preliminary study showed that sufficient spectral diversity can be expected within the bodies of already known but spectrally unclassified bodies.
The alternative plan is to start with a target from the current list and search for further reachable targets within the described selection constraints.

Table 2. Candidate asteroids for initial trajectory design.

Asteroid Name	Spectral Class (Tholen)	Diameter [km]
2048 Dwornik (1973 QA)	E	2.6
1920 Sarmiento (1971 VO)	X*	2.9
2491 Tvashttri (1977 CB)	X*	3.3
96177 (1984 BC)	D	3.4
2001 Einstein (1973 EB)	X*	4.0
1355 Magoeba (1935 HE)	X*	4.3

** Currently without known albedo to classify as E, M or P class*

3.5 ΔV - Budget

The ΔV - budget presented in Table 3 includes optional additional propellant which can be used if the preferred launch window is missed.

Table 3. Mass and ΔV budget by mission phase and propulsion type.

Mission Sequence	Wet Mass S/C (kg)	Prop Mass used (kg)	ΔV (m/s)	Type of Propulsion
Interplanetary Transfer				
Earth – Mars	4812	315.4	2660	Electric
Mars – Einstein	4496.6	1261.6	12921	Electric
Asteroid Hopping				
Transfer (all 4)	3235	1000	10569	Electric
Asteroid Visit				
Approach Phase (all 5)	2235	12	12	Chemical
Orbital Phase (all 5)	2223	160	260	Chemical
Total				
End of Primary Mission	2063	2749	26422	–

The Earth - Mars interplanetary section is the required propellant to get the desired gravity assist at Mars, from where we transfer to our first target; asteroid Einstein. The Transfer category lists an estimate propellant requirement to complete the 4 transfers to subsequent targets. The Approach phase lists the estimated propellant required for the maneuvers that are required to generate an initial shape model. The orbital phase lists the estimated propellant required to maintain a 1 km orbit around the target. The

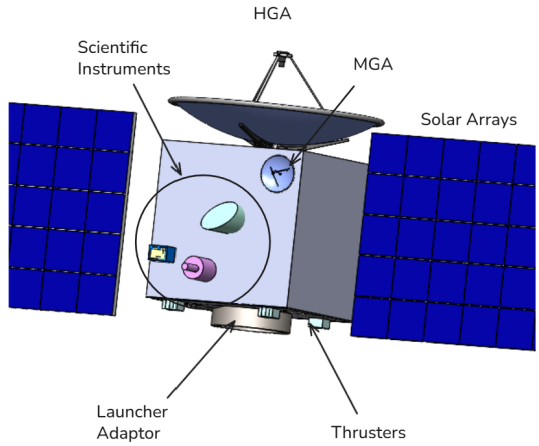

Figure 2. External view of the spacecraft.

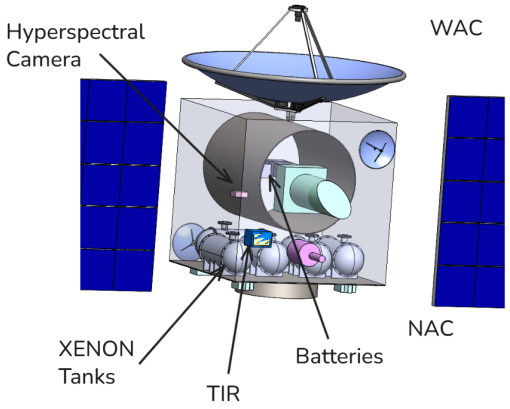

Figure 3. Internal layout of the spacecraft.

spacecraft has a dry mass of 1493 kg which means that this scenario has a surplus propellant of 570 kg. This is the mass of the optional additional fuel. If we make the desired launch window, this propellant will not be added to the spacecraft.

4 Spacecraft Design

4.1 Structure

The spacecraft primary structure consists of a cubic-shaped bus, as seen in Fig. 2, with dimensions of $2 \times 2 \times 2\text{m}^3$, formed by six square panels made of an Aluminum 5052-H39 honeycomb core (20 mm) and carbon fiber reinforced polymer (CFRP) skins (2 mm). It includes a central cylindrical CFRP structure (3.5 mm thick) extending from the launcher adapter, along with internal supports such as longerons to ensure integrity. The structure is designed to withstand mechanical loads during launch (−20 g to 20 g) and to accommodate all instruments, mechanisms and propulsion system. Spacecraft is expected to exceed minimum natural frequencies of 50 Hz for the first axial mode and 35 Hz for the first lateral mode while maintaining sufficient stiffness even with deployables. The placement of all the subsystems is shown in Figure 3. The structure is configured to ensure accessibility and to allow proper integration of the impactor mechanism at a later stage.

4.2 Propulsion

In order to perform the interplanetary transfer, we choose an electrical propulsion system with four thrusters positioned as a cross fashion. Two of which serve as redundancy in case one thruster becomes inoperant. The ArianeGroup RIT-2X radiofrequency ion thrusters are able to produce a thrust of 200 mN with a specific impulse (ISP) of 4000s at a power of 4650 W. In addition, their scalability at lower power, when the spacecraft will reach the main asteroid belt made them the most efficient choice for our mission. The ion thrusters are controlled and powered by two cross-strapped Thales power processing units Mk3. The thrusters use Xenon as a propellant, which is stored in five 60 L tanks (S-XTA-60 by MT Aerospace) pressurized at 187 bar.

4.3 Electrical Power System (EPS)

Solar Arrays

A solar array with two wings of five panels in cross-arrangement for a total surface of 90 m^2 provides up to 2.4 kW at 3 AU for end of life conditions (see Figure 4). The solar cells used, Azure 3G28, have successfully been used in low-intensity and low-temperate (LILT) environments in previous missions such as ESA's JUICE and NASA's Europa Clipper.

Power Control and Distribution Unit (PCDU)

The power generated by the solar array is handled by the off-the-shelf, space qualified and fault-tolerant AIRBUS PSR 100V MKII PCDU. Equipped with 8 power modules, the power capability of the PCDU is 11 kW - sufficient to distribute power to the S/C and two thrusters simultaneously, meeting the EPS requirements. The PCDU offers two managed battery slots, which will be occupied by Li-ion battery packs with a capacity of 144 Ah each.

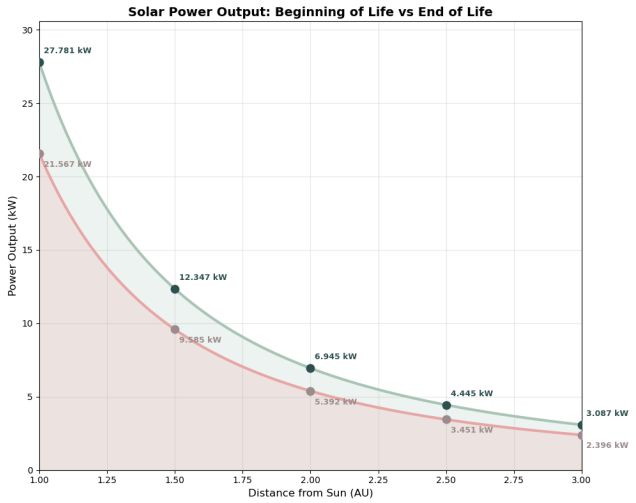

Figure 4. Beginning (green) and end of life (red) power generation from 1 AU to 3 AU. **Panel specifications**: 90 m^2, 28% nominal efficiency. **Packing factor**: 0.9. **Mission duration**: 10 years. **Degradation rate**: 2.5% per year.

4.4 Attitude Determination and Control System (ADCS)

Technical Overview

The ADCS subsystem was designed to perform 3-axis control. The attitude and orbital determination is accomplished using six sun

sensors (one on each side of the spacecraft), one miniature measurement inertial unit, and two star trackers (SODRA HYDRA) on two sides for accurate pointing. The actuators consist of four HR12-25 Reaction Wheels, arranged in a pyramid configuration (4th one for redundancy) and 12 hydrazine thrusters, distributed in two complete systems of 6 thrusters, for the de-saturation of the reaction wheels, accuracy of operations as well as redundancy. The combination of the specific models of the reaction wheels and the sun sensors was tested during the Lucy mission [8].

Pointing Mechanisms

The following pointing mechanisms are used to accomplish the pointing requirements during each operational phase of the mission:

- **Solar Panel Array**: A gimbaling mechanism is included in the solar panels' mounting interface, allowing them to rotate to face the sun.
- **High Gain Antenna**: The chosen high gain antenna (HGA) includes a gimbal that has two degrees of freedom.
- **Scientific Instruments**: All the scientific instruments are mounted on the same side of the spacecraft. The 3-axis control system will allow for them to point to the object of observation.
- **Medium Gain Antenna**: A steering mounting was chosen for the two medium gain antennas (MGA). However, they are mounted on two opposite sides of the spacecraft, allowing for a continuous communication window, even during tumbling of the spacecraft.

The described pointing mechanisms allow the simultaneous sun pointing, data downlink, and object observation during Science Mode.

4.5 On-Board Computer (OBC)

The OBC is based on Frontgrade's GR-SBC-GRG740 board. The board's processor GR740 has flown in missions and is on the European Preferred Parts List. The OBC is able to process data from all instruments. It is able to steer the S/C autonomously for ≥1.5 h, time in which ground station will be able to react to telemetry. It is radiation-hardened, and has a 1-out-of-2 warm redundancy. The mass storage is also radiation hardened and is based on ten UT81NDQ512G8T drives with total capacity 40 TB, allowing for generation of more data and selection of which will be downlinked, and providing redundancy.

4.6 Communications

Antennas

The communications system of the spacecraft consists of a single gimbaled high-gain antenna (HGA) with a diameter of 3 m, complemented by two steerable medium-gain antennas (MGAs), each 0.5 m in diameter. The HGA will be used during Downlink Mode for high-rate data transmission as well as for radio science, while the MGAs will be used during Transfer Mode and support housekeeping communications during Science Mode. All communication components selected for the mission have flight heritage from previous deep-space missions, such as Mars Reconnaissance Orbiter [15] and JUICE [35], demonstrating proven reliability.

Frequency Bands and RF Equipment

The HGA operates in Ka-band for high-rate science downlink and in X-band for command uplink. The MGAs use X-band. The spacecraft is equipped with a 70 W Ka-band traveling wave tube amplifier (TWTA) and a 100 W X-band TWTA.

4.7 Thermal Control System (TCS)

The thermal control strategy is based on both passive and active methods. For the passive approach, Multi-Layer Insulation (MLI) is used to cover the entire structure, keeping the platform as an isolated system, while passive radiators dissipate excess heat. However, since the temperature in the main asteroid belt is very low (175 K at 2.5 AU – 150 K at 3.5 AU), heaters are required for components that need a higher operational temperature. A basic thermal model, based on the Stefan-Boltzmann law, was used to estimate the radiator area required in the hot case scenario and the power needed for the heaters in the cold case scenario [21].

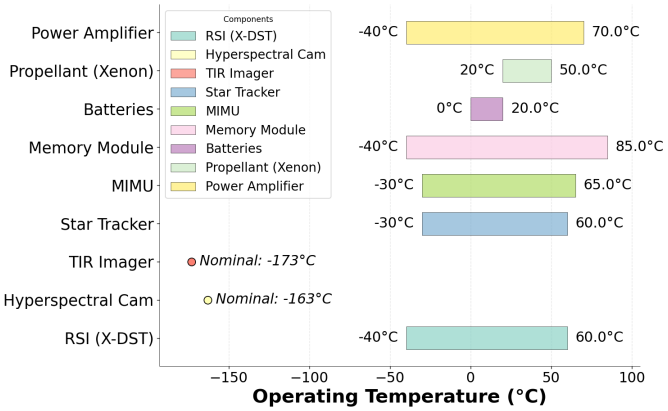

Figure 5. Temperature ranges of critical components.

Figure 5 provides a summary of the operating temperature ranges of critical spacecraft components. The hot case scenario considered for our mission occurs when the spacecraft is orbiting around the Earth, being the closest point to the Sun during the whole mission. In order to calculate the radiators area, four different heat fluxes were taken into account: sunlight from the Sun, albedo and infrared radiation from Earth, and the internal heat of the spacecraft. Figure 6 shows the result of this thermal analysis, being 12.5 m^2 the radiator area needed due to the maximum operational temperatures of the batteries.

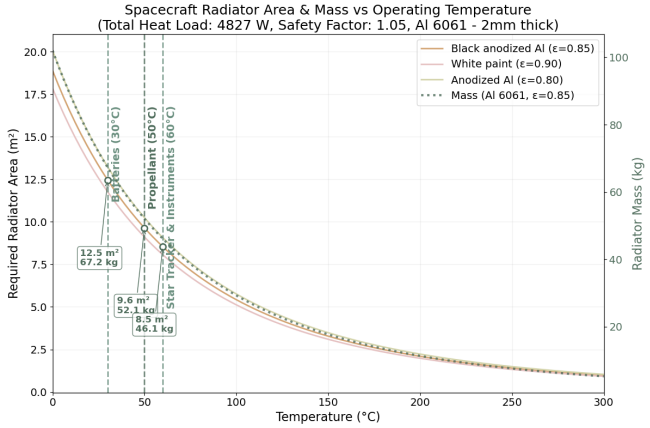

Figure 6. Radiators area with respect to critical temperature.

5 Budgets

5.1 Mass Budget

The total dry mass of the spacecraft is 1493 kg and the wet mass is 3693 kg. For the detailed breakdown, the reader is asked to look at Table 4. The margin philosophy that was applied is 5% for COTS components, 10% for modified components and 20% for components under development.

Table 4. Subsystem mass breakdown.

Subsystem	EPS	ADCS	OBC	COMMS	Prop.	TCS	ST	P/L	Total
Mass [kg]	490	249	21	108	137	110	311	67	**1493**

EPS: Electric Propulsion. ADCS: Attitude Determination and Control. OBC: On-board Computer. COMMS: Communications. Prop.: Propulsion. TCS: Thermal Control. ST: Structures. P/L: Payload.

5.2 Power Budget

Table 5 presents the nominal power consumption across all major subsystems for seven operational modes, with propulsion dominating during transfer mode. The payload becomes active in science mode and approach mode, while Safe Mode minimizes total power usage. These modes and transitions are designed to balance mission performance with power availability from the EPS, detailed in Section 8.

Table 5. Nominal power consumption per subsystem in each operational mode.

Subsystem	TM	IM	ScM	SM	DM	CM	AM
EPS	80	80	80	32	80	32	80
AOCS	95.4	173.4	147.4	43.72	169	0.72	169
OBC	19.5	19.5	19.5	7.8	19.5	7.8	19.5
COMMS	87.6	87.6	75.6	24	292	-	120
Prop.	9320	-	-	-	-	-	-
STC	10	10	10	5	10	6	10
TCS	100.7	100.7	100.7	60.4	100.7	-	100.7
P/L	-	-	96.275	-	-	-	18.515
Total [W]	**11656**	**565.4**	**635.4**	**207.5**	**805.4**	**55.8**	**621.2**

TM: Transfer Mode. IM: Idle Mode. ScM: Science Mode. SM: Safe Mode. DM: Downlink Mode. CM: Commissioning Mode. AM: Approach Mode.

5.3 Link Budget

The link budget is presented in Table 6, showing typical and worst-case values for uplink and downlink, where the worst-case corresponds to the data rates at the maximum distance between Earth and the spacecraft.

Table 6. Typical and worst-case data rates by antenna type, direction, and frequency band.

Antenna	Direction	Frequency Band	Data Rate (GB/h)	Worst Case (GB/h)
HGA	Uplink	Ka-band	1.3	0.225
	Downlink	X-band	0.18	0.036
MGA	Uplink	X-band	0.006	0.0011
	Downlink	X-band	0.0058	0.0009

5.4 Data Budget

See Table 7. The first table section is a low resolution model used for further decision-making. The second section is the main global model. The γ-ray and neutron spectrometer and RS antenna area also used in this model (output estimated by a different method as 0.61 GB). The third section is a high-resolution model of selected features, the fourth accounts for the re-imaging of parts of the surface after the use of the impactor. The budget makes some assumptions in addition to those in Ground Segment and Operations. The asteroid has 7 km diameter and is spherical. Image compression algorithms will remove any overlaps and compress the data losslessly 2.5:1, a typical ratio [7]. For comparison, the Rosetta mission collected 220 GB of data [12].

Table 7. Data budget for one asteroid.

Instrument	Required Resolution [px/m^2]	Pixel depth [bit/px]	Channels	Ratio of Area Imaged	Data Created [GB]	Downlink Time [days]
WAC	0.25	14	5	1	0.13	-
HS camera	1.78	12	128	1	21.02	2.03
TIRI	61.04	14	7	1	46.04	-
WAC	1.33	14	5	1	0.72	-
HS camera	1.78	12	128	1	21.02	6.57
HS camera	61.04	12	128	0.2	144.32	-
NAC	625.00	14	1	0.2	13.47	15.17
HS camera	61.04	12	128	0.2	144.32	-
NAC	625.00	14	1	0.2	13.47	15.17
TOTAL	-	-	-	-	404.50	38.89

6 Ground Segment and Operations

The mission uses ESA's 35 m deep space antennas, providing eight hours of daily contact. Telemetry (1500 bps) is transmitted in 0.11 seconds, while science data per asteroid (400 GB) requires 308 hours (38.5 days). Cebreros (Spain) is the primary ground station, with New Norcia (Australia) as backup. Science operations will be conducted by ESA's European Space Astronomy Centre (ESAC) in Spain, while mission operations will be managed by the European Space Operations Centre (ESOC) in Darmstadt, Germany.

7 Launcher

The mission will be launched aboard an Ariane 64, whose fairing provides a usable volume of 4.6 m diameter and 19 m height. Caelus, with a stowed configuration of 3 m diameter and 4 m height, fits well within these limits. The maximum allowed wet mass to achieve a $V_{infinity}$ of 3582 m/s is 4812 kg, which accommodates Caelus' current estimate of 3693 kg, including propellant margin. A PLA6 1194 interface ring has been selected, as it offers sufficient structural stability without interfering with the thrusters, which are mounted on the interfacing side of the spacecraft.

8 Concept of Operations

An overview of the concept of operations is illustrated in Figure 7. The operational modes are defined as:

Transfer Mode - Transfer between Earth and the Main Asteroid Belt, as well as between the asteroids. It is the most power demanding mode, being the most critical constraint.

Approaching Mode - Initial mapping of the objects, to achieve a stable orbit around the asteroid.

Idle Mode - Default mode in which the spacecraft is sun pointing to get the highest possible generated power and prepare for new commands.

Science Mode - Divided into 3 phases:

1. **Phase 1 - Detailed surface mapping**: Initially the detailed mapping of the object's surface is performed, lasting 20-25

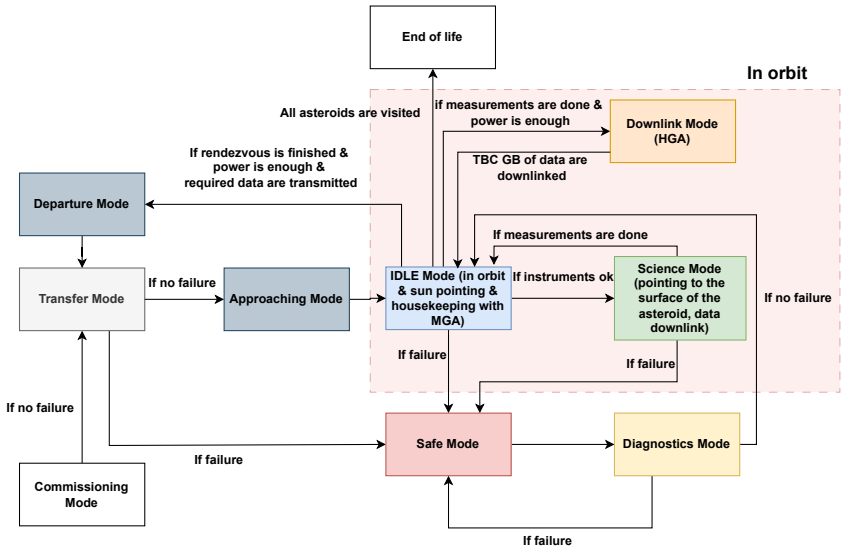

Figure 7. Concept of Operations.

days. A low amount of low resolution data is downlinked and, after the determination of the high interest areas, the detailed mapping of those areas is commanded by the Ground Station.

2. **Phase 2 - Impact**: The spacecraft rotates 180 degrees, pointing the impactor to the surface of the object and the instruments on the opposite side. As soon as the attitude is stabilized, the impact is performed and the spacecraft remains in the same attitude for half an orbit, avoiding potential debris caused by the impact.
3. **Phase 3 - Post impact Observation**: The surface of the crater is mapped.

During the whole duration of the Science Mode, high resolution data is downlinked with the HGA, which can be pointed individually thanks to the gimbal system:
Downlink Mode - Post Science Mode, the remaining data is downlinked with the HGA.
Departure Mode -Preparing to depart from the observed object and transfer to the next one, based on the mission design.
Safe Mode - The spacecraft enters the safe mode (SM) with 3 types of triggers for critical failures, which are power failure, temperature failure, stabilization failure (tumbling). Failure detection, isolation and recovery is performed and the following actions are implemented

1. Stabilization of the spacecraft
2. Sun Pointing
3. Communication with the Ground Station (MGA)

Diagnostics / Engineering Mode - After the recovery during the safe mode, a transition to this mode is triggered, for detailed diagnostics on all of the subsystems for failure detection and identification. The instruments are also calibrated.

9 Mission Drivers

The key mission drivers of the Caelus Mission are

- Asteroid classification pre-survey
- Impactor development, test and verification plan
- Successful downlink of the data
- Detailed trajectory analysis
- Detailed thermal profile for the whole mission duration
- Refinement of in-orbit operations

10 Risk Assessment

Mission Success Criteria: We deem the mission a success if we receive hyperspectral data, shape models and mass measurements of at least three asteroids of different classes.
Science and Operational Risks: The following Tables 9 and 8 outline technical and scientific risks identified for the Caelus mission, alongside corresponding mitigation strategies. The risks are ordered by increasing probability (bottom to top). The technical risks covers operational or design issues like launch delays, communication limits, or thruster failures, while the scientific risks captures mission science threats such as asteroid surface conditions or failure to obtain usable subsurface data. The risk assessment score can be compared with the matrix key in Figure 8.

Figure 8. Risk assessment key.

Table 8. Scientific risks and mitigation strategies.

Risk	Matrix	Mitigation
Asteroid surface is covered by dust	P1/S3	Relax science requirements (e.g., L0-020-MO)
Asteroid shape does not allow for safe operations at 1 km	P2/S2	Conduct observations at distances > 1 km
Impactor fails to excavate sufficient unaltered material	P2/S1	Redundant impactor projectile

Table 9. Technical risks and mitigation strategies.

Risk	Matrix	Mitigation
Construction delay – missed launch window	P2/S2	Flexible targets
Unexpected costs / low budget	P2/S2	Descope to Ariane 62
Insufficient downlink speed	P2/S1	1. Less data transmitted but still partial success 2. Possibility of utilizing a second ground station antenna
Impact-generated debris affects performance	P1/S3	1. Instruments do not face the impact direction 2. Solar panels can be rotated
Thruster failure	P1/S3	Redundant 3rd & 4th thrusters
OBC radiation damage	P1/S2	OBC resists 500 Gy total dose and single-event latchup

11 Trade Off Study

11.1 De-scoping options

To achieve adaptation and mission agility, Caelus Mission can be de-scoped to become compatible with Ariane 62, which supports up to 2600 kg for Earth-escaping orbits without modification. This requires lowering the number of mission targets from five to three and de-scoping several elements, saving 1105–1150 kg. However, the enhanced scientific return of the full configuration on Ariane 64 is considered to justify the additional cost and risk compared to the descoped option.

11.2 Scalability

The mission design allows for potential extension beyond the nominal phase, depending on available fuel, and downlink capacity. Possible extended mission activities include additional rendezvous with new targets (including a potential impactor operation), increased orbital time around the final asteroid for enhanced surface investigation, and further flybys of other objects, all contributing to increased scientific return.

12 Project Planning

12.1 Development Plan

The development plan for the Caelus Mission is shown in Fig.,10.

Table 10. Mission Phases with Duration.

Phase	Contents	Duration (years)
Phase 0	Proposal	1
Phase A	Feasibility Analysis	1
Phase B1/B2	Preliminary Design	3
Phase C/D	Design & Development activities, MAIT/MAIV	7
Phase E	Launch Campaign & Launch Window, Operations	10
Phase F	Disposal	-

12.2 Open points

The asteroid sequence must be finalized. The first asteroid has been chosen and the following ones must share similar orbital parameters to optimize the "hopping" sequence. A preliminary study has been conducted, and we believe that a method using an angular momentum-based tree search with a nearest-neighbor scheme and nonlinear optimization algorithm would produce the best sequence results. Then, the trajectory between the asteroids of the sequence must be computed using a Lambert transfer approach using ephemeris-level accuracy. The End-of-Life (EoL) strategy also remains to be defined.

For the impactor, ground tests could increase the TRL from 3 to 5. 3-axis pointing and barrel alignment must be verified. Recoil effects on spacecraft dynamics will be modeled, and mitigation strategies (e.g. gas vents, AOCS) explored. Crater ejecta dynamics require improved estimation.

13 Cost Estimate

The total mission cost has been estimated using a rough order of magnitude (ROM) approach based on ESA experience. The table below summarizes the breakdown, including Cost at Completion (CaC), launcher, and payload. Payload costs are expected to be covered by ESA Member States. Overall, the mission remains within the cost envelope of an ESA L-class mission.

Table 11. ROM cost breakdown for Caelus mission.

Item	Percent	Cost
Project Team	9%	70 M€
Industrial Costs	40–50%	350 M€
Mission Operations Centre (MOC)	5–10%	80 M€
Science Operations Centre (SOC)	5–10%	70 M€
Contingency	20%	114 M€
Cost at Completion (CaC)	**100%**	**684 M€**
Launcher (Ariane 64)		131 M€
ESA Cost		**815 M€**
Payload (ESA member states contribution)		250 M€
Total (with payload)		**1,065 M€**

14 Conclusion

The Caelus mission proposes the investigation of multiple types of asteroids in the main belt. Equipped with cameras, radio science technology, gamma-ray & neutron detector and an impactor, Caelus will provide insights into the surface and internal structures of the observed asteroids as well as in its composition. Consequently, valuable connections between formation processes in the early solar system, age and different asteroid types can be made. One can say, this mission will undoubtedly enrich our current knowledge about asteroids and their evolution since the formation of our Solar System.

Acknowledgements

We would like to express our sincere gratitude to FFG, ESA and Austrospace for organising the Alpbach Summer School 2025. We thank all tutors for their valuable guidance and support throughout this project.

Special thanks to our engineering tutor ***Christian Gritzner*** *(Deutsches Zentrum für Luft- und Raumfahrt) for his technical insights, and to our science tutor* ***Peter Woitke*** *(Austrian Institute for Space Research) for his scientific expertise and mentorship. We also want to extend our thanks to* ***Marcus Hallmann*** *for his help and guidance about mission design questions and trajectory analysis.*

References

[1] Al Asad, M. M., Philpott, L. C., Johnson, C. L., et al. 2021, Planet. Sci. J., 2, 82, publisher: American Astronomical Society

[2] Arakawa, M. e. a. 2020, Science, 368, 67

[3] Bernardi, P., Reess, J.-M., Castelnau, M., et al. 2024, in Space Telescopes and Instrumentation 2024: Optical, Infrared, and Millimeter Wave, ed. L. E. Coyle, S. Matsuura, & M. D. Perrin, Vol. 13092, International Society for Optics and Photonics (SPIE), 130922J

[4] Bottke, W. F., Durda, D. D., Nesvorný, D., et al. 2005, Icarus, 175, 111

[5] Chapman, C. R. 1994, in IAU Symposium, Vol. 160, Asteroids, Comets, Meteors 1993, ed. A. Milani, M. di Martino, & A. Cellino, 357

[6] Cheng, A. F., Agrusa, H. F., Barbee, B. W., et al. 2023, Nature, 616, 457

[7] Consultative Committee for Space Data Systems. 2022, Low-Complexity Lossless and Near-Lossless Multispectral and Hyperspectral Image Compression, Tech. Rep. CCSDS 120.2-G-2, CCSDS, accessed: 2025-07-16. See pp. 6-7 to 6-11

[8] Cox, M., Dworkin, J., Levison, H., et al. 2025, The Lucy Spacecraft, Tech. Rep. NASA/TP–20250001468, NASA Goddard Space Flight Center, available at https://ntrs.nasa.gov/citations/20250001468

[9] Dibb, S. D., Asphaug, E., Bell, J. F., et al. 2024, AGU Advances, 5, publisher: American Geophysical Union (AGU)

[10] El Mir, C., Ramesh, K., & Delbo, M. 2019, Icarus, 333, 356

[11] ESA. 2004, European Code of Conduct for Space Debris Mitigation (ESA)

[12] European Space Agency. 2020, Rosetta, accessed: 2025-07-16

[13] Gramigna, E., Lasagni Manghi, R., Zannoni, M., et al. 2024, Planet. Space Sci., 246, 105906

[14] Grott, M., Knollenberg, J., Hamm, M., et al. 2019, Nat. Astron., 3, 971

[15] Johnston, M. D. & Ilott, R. R. 2005, in Deep Space Communications and Navigation Series (JPL DESCANSO Monograph Series), 1–56, accessed: 2025-07-16

[16] Keil, K. 2000, Planet. Space Sci., 48, 887, asteroids, Comets, Meteors (ACM) Conference

[17] Keil, K. 2000, Planet. Space Sci., 48, 887

[18] Kohout, T., Čuda, J., Filip, J., et al. 2014, Icarus, 237, 75

[19] Kovács, G., Nathues, A., Sierks, H., et al. 2024, Space Sci. Rev., 220, 4

[20] Kruijer, T. S., Kleine, T., & Borg, L. E. 2020, Nat. Astron., 4, 32

[21] Larson, W. J. & Wertz, J. R. 2005, Space Mission Analysis and Design, 3rd edn. (Microcosm Press and Kluwer Academic Publishers)

[22] Lauretta, D. S., Balram-Knutson, S. S., Beshore, E., et al. 2017, Space Sci. Rev., 212, 925

[23] MacLennan, E. M. & Emery, J. P. 2021, Planet. Sci., 2, 161

[24] Moretti, P., Maras, A., & Folco, L. 2007, Adv. Space Res., 40, 258

[25] Neumann, W., Grott, M., Trieloff, M., et al. 2021, Icarus, 358, 114166

[26] Neumann, W., Luther, R., Trieloff, M., Reger, P. M., & Bouvier, A. 2023, Planet. Sci. J., 4, 196

[27] Okada, T. 2024, in 45th COSPAR Scientific Assembly., Vol. 45, 178

[28] Palumbo, P., Roatsch, T., Lara, L. M., et al. 2025, Space Sci. Rev., 221, 32

[29] Patzek, M. & Rüsch, O. 2022, J. Geophys. Res. Planets, 127, e2022JE007306, e2022JE007306 2022JE007306

[30] Prettyman, T. H., Feldman, W. C., McSween, H. Y., et al. 2011, Space Sci. Rev., 163, 371

[31] Prockter, L., Murchie, S., Cheng, A., et al. 2002, Acta Astronaut., 51, 491

[32] Richardson, J. E., Steckloff, J. K., & Minton, D. A. 2020, Icarus, 347, 113811

[33] Russell, C. T. & Raymond, C. A. 2011, Space Sci. Rev., 163, 3, publisher: Springer Science and Business Media LLC

[34] Saiki, T., Imamura, H., Arakawa, M., et al. 2015, Space Sci. Rev., 208, 165

[35] SENER Aerospace and Defense. 2022, JUICE's Medium Gain Antenna Subsystem (MGAMA), accessed: 2025-07-16

[36] Shepard, M. K., de Kleer, K., Cambioni, S., et al. 2021, Planet. Sci. J., 2, 125

[37] Taylor, M. G. G. T., Altobelli, N., Buratti, B. J., & Choukroun, M. 2017, Philos. Trans. R. Soc., A, 375, 20160262

[38] Tsiganis, K., Gomes, R., Morbidelli, A., & Levison, H. F. 2005, Nature, 435, 459

[39] Vernazza, P., Ferrais, M., Jorda, L., et al. 2021, A&A, 654, A56

[40] Walsh, K. J., Ballouz, R. L., Bottke, W. F., et al. 2024, Nat. Commun., 15, 5653

[41] Walsh, K. J., Morbidelli, A., Raymond, S. N., O'Brien, D. P., & Mandell, A. M. 2011, Nature, 475, 206

[42] Watanabe, S.-i., Tsuda, Y., Yoshikawa, M., et al. 2017, Space Sci. Rev., 208, 3

[43] Woitke, P., Drążkowska, J., Lammer, H., Kadam, K., & Marigo, P. 2024, A&A, 687, A65

[44] Youdin, A. N. & Goodman, J. 2005, Astrophys. J., 620, 459

[45] Zannoni, M., Tommei, G., Modenini, D., et al. 2018, Adv. Space Res., 62, 2273

[46] Zhang, P., Tai, K., Li, Y., et al. 2022, A&A, 659, A78